JOURNAL OF MATERIALS SCIENCE, 33 (1998) 817–826

Phase transformations in a welded near-α titanium alloy as a function of weld cooling rate and post-weld heat treatment conditions

K. KESHAVA MURTHY, S. SUNDARESAN
Department of Metallurgical Engineering, Indian Institute of Technology, Madras 600 036, India

In α-β titanium alloys, the high-temperature β phase can decompose in several ways, depending on alloy composition and cooling rate. In the case of welded joints, cooling rates can vary widely as a function of heat input. In the current work, a dilute α-β Ti-Al-Mn alloy was welded over a range of heat inputs using electron beam and gas tungsten-arc welding processes. A major part of the rapidly cooled electron beam weld could be identified as lath-type or "massive" martensite. In the slower cooled gas tungsten-arc welds, the transformation product was a mixture of lamellar α and β phases formed entirely by diffusion. Post-weld heat treatment resulted, in all cases, in an α-β structure that coarsened with annealing temperature and time. Tensile elongation in the as-welded condition was poor on account of a large prior-β grain size and an acicular microstructure. The ductility improved as the structure coarsened on heat treatment. Tensile fracture was always microscopically ductile, but the presence of a grain boundary α layer tended to induce intergranular rupture, especially when a hard, intragranular matrix confined slip to occur in the grain boundary regions. © *1998 Chapman & Hall*

1. Introduction

The decomposition of the high-temperature β phase in α-β titanium alloys may take place in several ways depending on alloy chemistry and cooling rate. The phase transformation could occur by diffusion or shear or by a combination of both [1]. While the diffusional transformation may occur through several modes of α nucleation and growth, the product of the shear transformation (α′) may also be either a plate-type martensite or a lath-type martensite.

The transformation to lath-type martensite, which has been sometimes referred to as massive martensite [2], is more likely to occur in rapidly-cooled dilute alloys. According to Flower and co-workers [2], the high M_s temperature favours slip in the β phase ahead of the α′ plate that reduces the shape strain of the martensitic transformation; diffusion, also facilitated by the high temperature, may make a further contribution to the relief of shape strain. In very dilute alloys the critical cooling rate may not be achieved even during water-quenching and competitive shear and diffusional transformations could take place [3]. The transition from diffusional to shear growth, or vice versa, is not sharply defined, since the h.c.p. phase formed by diffusion exhibits the same habit plane and the same orientation relationship with the β phase as that which forms by shear [2].

During welding of α-β titanium alloys, solidification in the fusion zone occurs epitaxially as β crystals, which cool further at a rate determined primarily by the heat input, i.e. the energy delivered per unit length of weld. Previous work on several α-β titanium alloys has shown that laser beam [4] and electron beam [5] welds, which are characterized by a low heat input and consequently rapid cooling rate, exhibit a predominantly martensitic structure in the weld metal; while slower cooled gas tungsten-arc welds contain a much larger proportion of the diffusional α phase [6]. The formation of "massive" martensite during welding has been confirmed by Baeslack and Mullins [7], who demonstrated the presence of both lath and plate martensite in the fusion zone of a near-α titanium alloy.

The transformations during continuous cooling could thus be quite complex, particularly in alloys lean in β stabilizer content. Since cooling rates in welding also vary depending on welding conditions, a wide spectrum of microstructures may be expected to form in the fusion zone. This will obviously have an important effect on the properties of the weldment.

Fusion zones in welded α-β titanium alloys are known to exhibit poor ductility that is usually attributed to a large prior-β grain size and a wholly or partially martensitic microstructure of high aspect ratio. The situation cannot be remedied with a change of heat input alone and a post-weld heat treatment is required for restoring ductility. This is a particularly serious problem in the use of high-strength α-β alloys, which in the unwelded condition can be processed to possess greater fracture toughness than the widely-used Ti–6Al–4V. This has led to the development, for

structural applications, of a class of relatively dilute α-β titanium alloys having moderate strength but appreciably greater ductility that would ensure adequate weldability.

The current paper is concerned with one such medium-strength α-β Ti–Al–Mn alloy of low solute content corresponding to the Russian specification OT4-1. This was welded using a range of heat inputs by electron beam and gas tungsten-arc welding. Different post-weld heat treatments were subsequently applied. The paper discusses the structural changes that occur during welding and during subsequent thermal treatments and their effects on tensile properties of the fusion zone.

2. Experimental procedure

The base material used was a 5 mm thick sheet of OT4-1 alloy with the following composition (wt %): Al 2.6; Mn 2.2; Si 0.018; Fe 0.03; Ni 0.006; Zr 0.003; C 0.006; H 0.002; O 0.113; N 0.010; Ti balance. It was received in the α-β processed and annealed condition. Since energy input and cooling rate during welding were important considerations, welding was carried out using different processes: electron beam welding (EBW); automatic gas tungsten-arc welding (A-GTAW); and manual gas tungsten-arc welding (M-GTAW). M-GTAW was performed in a hemispherical "glove-box" of 1 m diameter in which a positive pressure of high-purity argon was maintained. For A-GTAW, auxiliary trailing and backing shields were used in addition to the torch gas. The degree of vacuum in EBW corresponded to 1.333×10^{-3} Pa. The welding conditions used for all the three processes are given in Table I. Autogenous full-penetration bead-on-plate welds were made on strips cut from the sheets.

For the post-weld heat treatment of α-β titanium alloys, an upper temperature limit is set by the β-transus. This was experimentally determined as the lowest solution treatment temperature from which on quenching a fully lamellar structure was obtained. The β-transus for the alloy was thus established to be 920 °C. One post-weld heat treatment was conducted at 870 °C, because earlier work had shown that such treatment at a temperature high in the α-β region is required for conferring an adequate improvement in ductility [6]. Another post-weld annealing treatment was carried out at 700 °C, which is in the usual stress-relieving temperature range for such alloys, to see if it would result in sufficient improvement over the as-welded condition. Both the above treatments were followed by furnace cooling. Welded strips were also subjected, as occasionally recommended in the literature [4], to a duplex annealing treatment according to the schedule: 870 °C–3 h/furnace cool (FC) + 650 °C–3 h/FC. All heat treatments were performed in a vacuum furnace at a pressure of 1.33×10^{-3} Pa.

Metallographic examination was carried out using light and transmission electron microscopy. Thin foils for the latter were prepared by twin-jet electropolishing using a solution containing 6% H_2SO_4 and 94% methanol.

The tensile properties were evaluated using longitudinal welded specimens, i.e. with the weld length oriented along the loading axis. The tests were carried out in a 100 kN servohydraulic machine at a cross-head speed of 0.5 mm min^{-1}. The tensile fracture faces were examined using a scanning electron microscope. Hardness profiling across the weld metal was performed by making Vicker's hardness measurements with a 5 kg load.

3. Results and discussion

The microstructure of the base material shown in Fig. 1 consists of equiaxed α grains within a grain

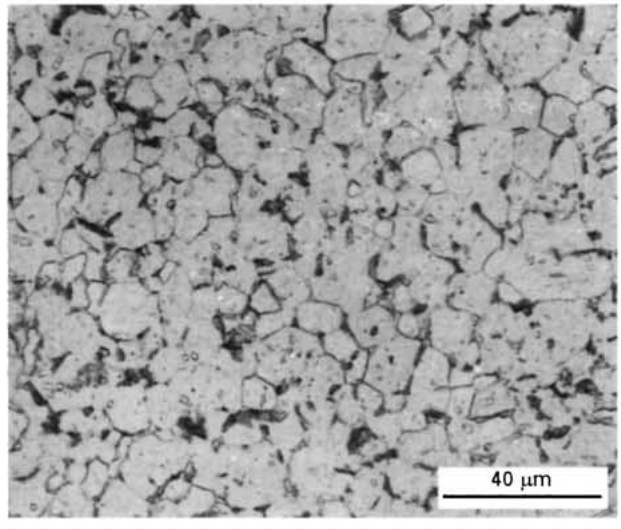

Figure 1 Light micrograph of the base material.

TABLE I Welding parameters for electron beam, automatic GTA and manual GTA welding of OT4-1 alloy

Process	Arc/beam voltage (V)	Arc/beam current (A)	Travel speed (mm min^{-1})	Heat input (J mm^{-1})
Electron beam welding	100×10^3	52×10^{-3}	2400	130
Automatic GTAW	12	170	220	556
Manual GTAW	14	190	170	939

Other parameters:
Electron beam welding: Vacuum of 1.333×10^{-3} Pa.
Automatic GTAW: Torch gas flow rate = 7 l min^{-1}
Trailing gas flow rate = 14 l min^{-1}
Backing gas flow rate = 5 l min^{-1}
Manual GTAW: Torch gas flow rate = 10 l min^{-1}

boundary network of the β phase, the latter being small in amount on account of the low manganese content in the alloy.

3.1. As-welded microstructures

In the fusion zone macrostructures given in Fig. 2a–c, the differences in prior-β grain size are clearly seen, reflecting the differences in cooling rates. The EB weld, characterized by a rapid rate of heating but a low total heat input (see Table I), cools much faster than the two GTA welds. It has been reported [8] that the three processes may be characterized by approximate cooling rates of 550 °C s^{-1} (EBW), 60 °C s^{-1} (A-GTAW) and 15 °C s^{-1} (M-GTAW). The M-GTA weld experiences the slowest cooling and exhibits the coarsest grain structure.

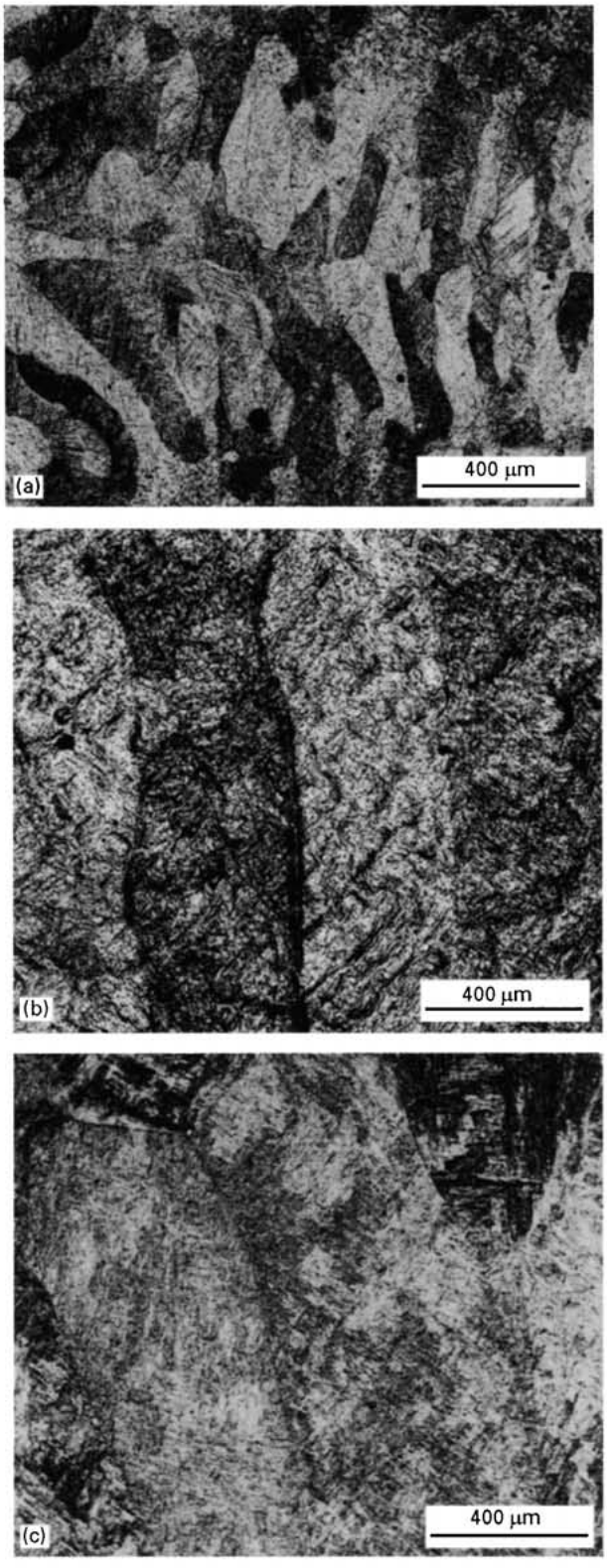

Figure 2 Macrostructures of the weld metal: (a) electron beam weld; (b) automatic GTA weld; (c) manual GTA weld.

The microstructures of transverse sections of the three weld metals are given in Fig. 3a–d. The EB weld in Fig. 3a shows a sharply needle-like microstructure with no evidence of any α phase formation at the prior-β grain boundary. The A-GTA weld (Fig. 3b), cooling more slowly than the EB weld, shows a slightly greater intragranular coarsening. The lower magnification photograph (Fig. 3c) reveals more clearly α side-plates emanating from the grain boundaries and a fine basketweave Widmanstätten structure in the grain interior. Grain boundary α allotriomorphs were present but only in isolated regions of the microstructure. The M-GTA weld, on the other hand, shows a clear grain boundary α network which, however, is still quite thin and discontinuous (Fig. 3d). α side-plates growing in from the grain boundaries are also observed as in the A-GTA weld.

Fig. 4a and b are transmission electron micrographs of the parent material water-quenched from 1050 °C. Fig. 4a shows primary α plates, many of them parallel-sided, partitioning the prior-β grains, with a number of secondary plates of varying size and orientation formed within the partitioned regions. The colony type of parallel-plate arrangement is more clearly observed in Fig. 4b. The electron micrographs of the EB weld metal given in Fig. 5a and b also reveal a mixture of primary and secondary plates, with much of the α phase appearing as a colony product of parallel plates. The similarity in the structures of the water-quenched and electron beam welded specimens is clearly visible. In several of the colony α plates in both cases dislocations were observed.

Transmission electron micrographs of the two GTA welded specimens (Fig. 6a and b) show only parallel α plates separated by thin strips of β phase, with no evidence of any lenticular plates. Also, the average α plate width is seen to be slightly lower in the A-GTA weld (0.44 μm) than in the more slowly-cooled M-GTA weld (0.61 μm).

In all the three welded specimens, as well as in the water-quenched base material specimen, selected area diffraction revealed the presence of the β phase, implying the occurrence of diffusion to a greater or smaller degree in all cases. Semiquantitative scanning tunnelling electron microscopy (STEM) analysis yielded additional confirmation by showing that the beta phase was enriched in manganese and depleted in aluminium in relation to the hexagonal phase.

The β phase is thus seen to exist not only in the GTA welds but also in the EB welds and during water quenching. This means that, in the latter two cases, although cooling is sufficiently rapid not to permit appreciable long-range atomic migration (as evidenced, for example, by the absence of grain boundary α), still there has been some diffusional contribution to the transformation. This is also reflected in the fact

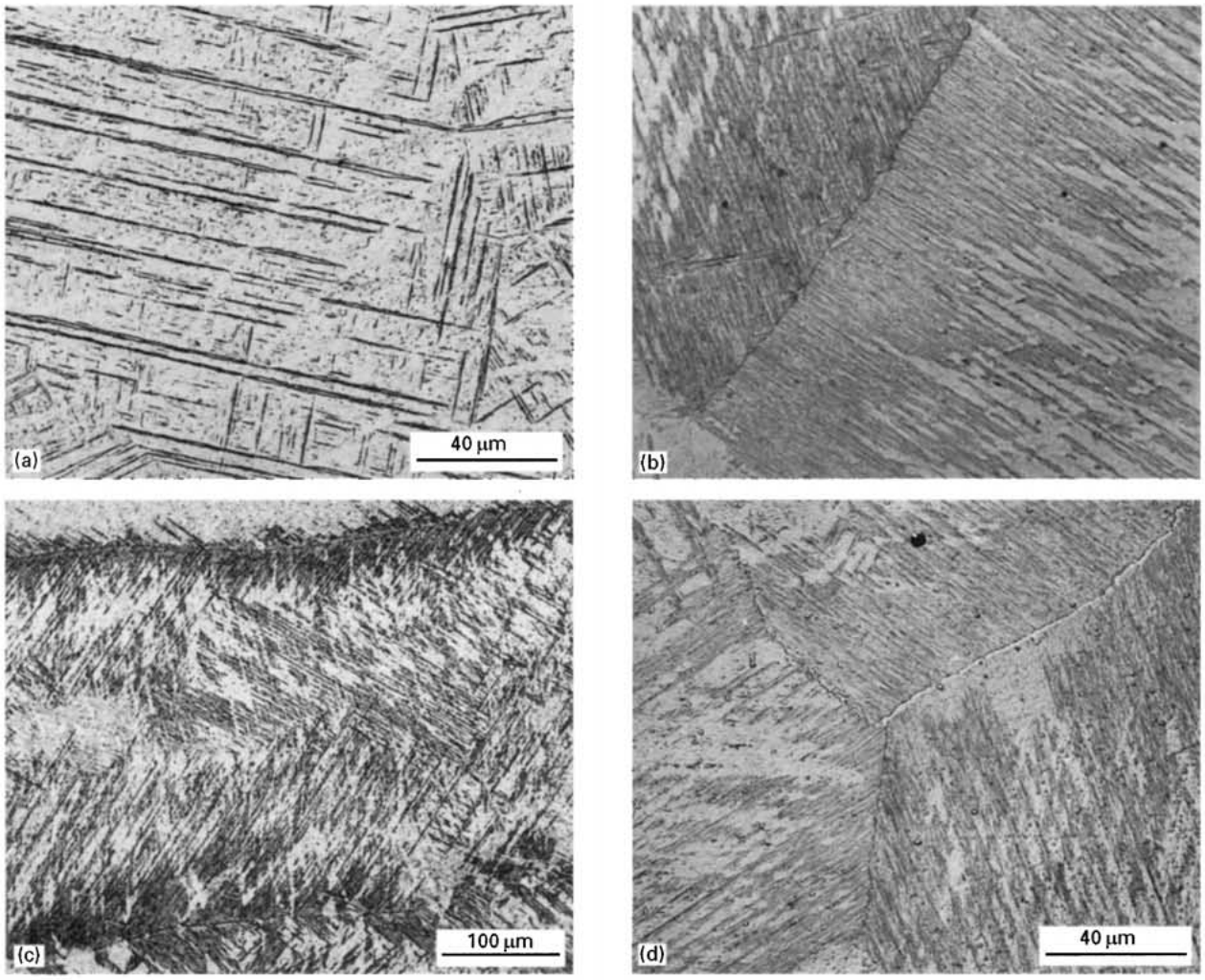

Figure 3 Light micrographs of transverse sections of fusion zone, as-welded condition: (a) electron beam weld; (b) and (c) automatic GTA weld; (d) manual GTA weld.

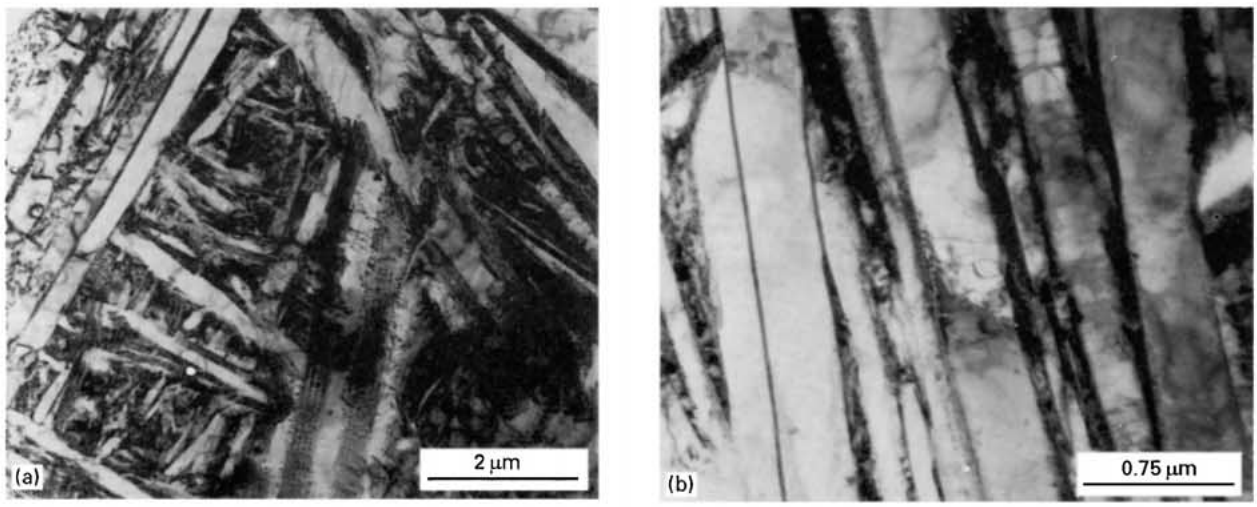

Figure 4 (a, b) Transmission electron micrographs of the base material water-quenched from the β phase field.

that, on account of the low solute content in the alloy, the time–temperature transformation (or continuous cooling transformation) diagram for completely diffusional β decomposition may be expected to lie close to the temperature axis, so that even during water quenching or electron beam welding some diffusion-aided reaction might occur. The occurrence of diffusion is further explained by the high diffusion coefficient of manganese. According to Zwicker [9], manganese diffuses in β titanium eight times as fast as vanadium and niobium, which in turn diffuse faster than molybdenum. The role played by diffusion in the

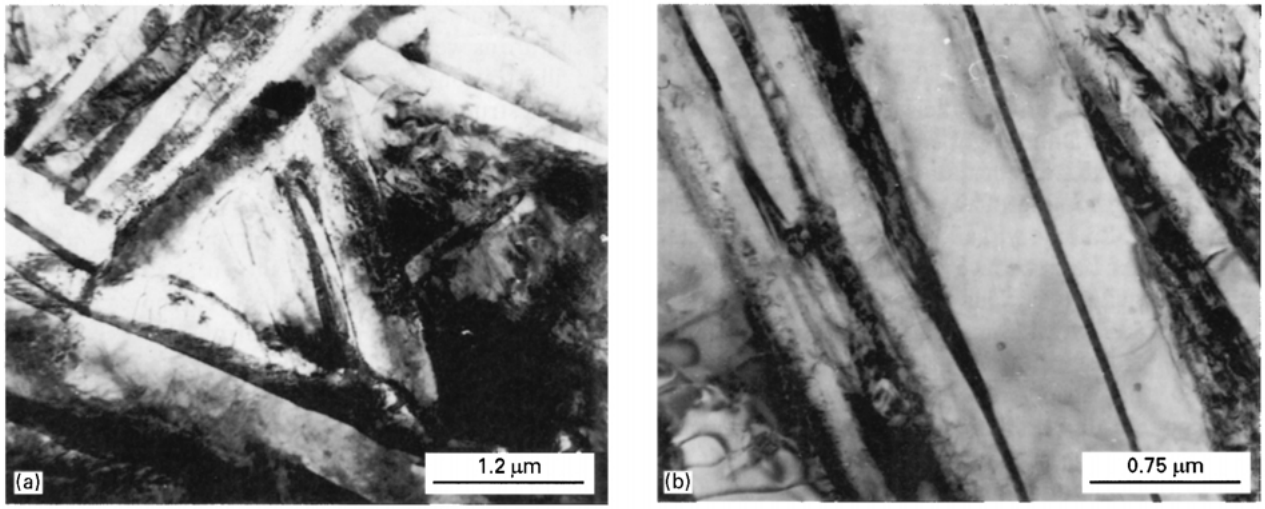

Figure 5 (a, b) Transmission electron micrographs of electron beam weld, as-welded condition.

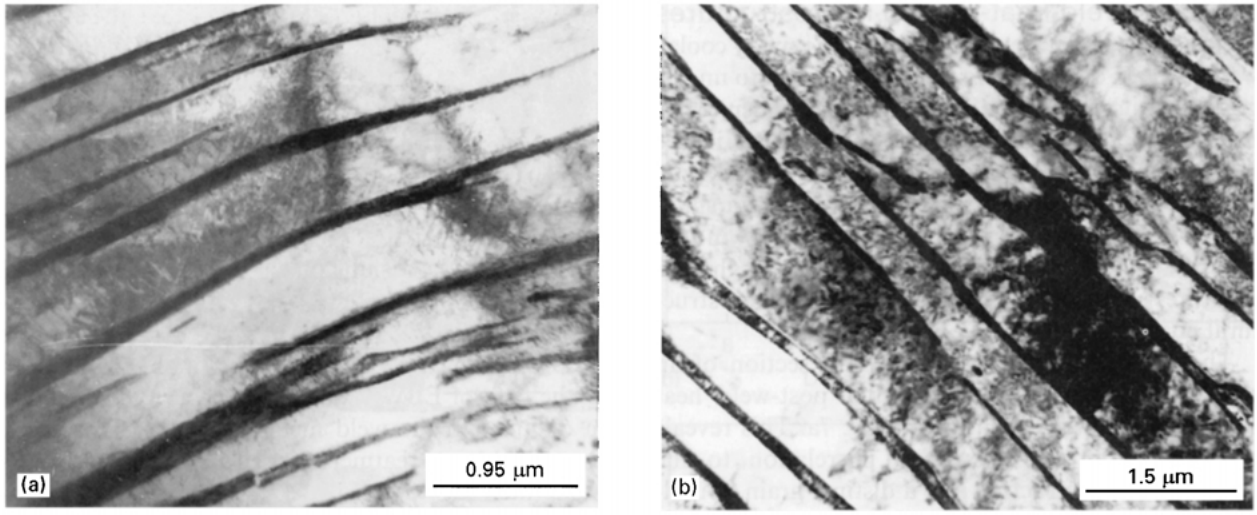

Figure 6 Transmission electron micrographs of the two GTA welds: (a) automatic GTA weld; (b) manual GTA weld.

transformation, the formation of parallel α plates as colonies and the presence of dislocations in several of the α plates suggest that the colony product obtained in water quenching and in EB welding may be predominantly lath-type or "massive" martensite. The formation of "massive" martensite in dilute α-β titanium alloys is well known [2, 3].

The transformation to "massive" martensite is directly related to the high M_s temperature of the alloy resulting from its low solute content. High M_s temperatures are known to favour transformation to "massive" martensite. It has been suggested that the lattice invariant shear in "massive" martensite occurs by internal slip [10]; according to Flower *et al.* [11], "massive" martensite forms when slip takes place in the β phase ahead of the α prime plate to reduce the shape strain. This is followed by the growth of more α prime plates next to the first and exhibiting parallel orientation. It has been further suggested that diffusion following the initial growth of the shear plates may also help in reducing the shape strain [2]. The significant role played by diffusion in the formation of "massive" martensitic structures in Ti–Mo and other titanium alloys has been highlighted by Davis and co-workers [3]. It is obvious that both slip and diffusion will be encouraged by the low alloy content as in the present case, which results in the transformation occurring at high temperature.

In Fig. 4a randomly oriented lenticular plates of martensitic α prime phase are seen to infill the regions partitioned by the primary plates of the colony product. This indicates that the acicular martensite has formed at lower temperatures than the lath-type martensite. This is understandable because at the lower temperatures diffusion is more difficult and the β phase is also strengthened sufficiently to resist slip.

The microstructures of the GTA welds (Figs 3b and d and 6a and b and reveal the increasing contribution of diffusion when cooling rate is reduced. There is greater intragranular coarsening, growth of a large number of parallel α side-plates from the grain boundaries and an α phase layer outlining the prior-β grain boundaries. However, there is no acicular martensite in any of these structures. It is apparent that, as cooling becomes slower, the transformation occurs entirely under diffusion control to yield a lamellar

product consisting of α plates separated by thin strips of the β phase.

The transformation of the β phase, as a function of cooling rate, has many parallels to austenite decomposition in steels. Damkroger *et al.* [12] have identified four individual transformation products that could result during cooling of the β phase in α-β titanium alloys: grain-boundary α allotriomorphs, α side-plates, intragranular basketweave Widmanstätten structures and martensite. It is clear that, as the cooling rate is increased and transformation temperature is lowered, the latter transformations are encouraged at the expense of the earlier ones. Thus, all three diffusional products are noticeable in the two GTA welds, and a predominantly martensitic structure is formed in the EB weld. The grain boundary α layer is also more distinctly developed in the M-GTA weld in relation to that in the A-GTA weld which cools relatively faster.

3.2. Post-weld heat-treated microstructures

Metastable microstructures produced in rapidly cooled weldments in α-β titanium alloys are known to undergo two important reactions during subsequent thermal treatment: (1) formation of the β phase in the martensite which thus reverts to the equilibrium α phase on account of the lowering of the beta stabilizer content; (2) precipitation of α phase in the retained β [6]. Prolonged heat treatment at high temperatures results in overageing effects and microstructural coarsening.

The microstructure of a transverse section of an electron beam weld obtained after post-weld heat treatment at 700 °C is shown in Fig. 7a. This reveals some intragranular coarsening in relation to the as-welded microstructure and a distinct grain boundary α layer. Microstructures of the two GTA welds after treatment at 700 °C were similar to Fig. 7a, showing that microstructural differences in the as-welded condition get substantially eliminated even in the 3-h treatment at 700 °C. When the temperature of treatment is increased to 870 °C, both for the single and duplex anneals, the coarsening became much more prominent, for the intragranular basketweave structure as well as for the grain boundary α phase. As an illustration of these high-temperature post-weld treated structures, Fig. 7b shows the microstructure of an electron beam weld heat-treated at 870 °C. Microstructures of the other high-temperature treated welds were similar to these.

The transmission electron micrographs of the post-weld heat treated material, shown as an example in Fig. 8a–c for the M-GTA weld, reveal more clearly the differences in α plate growth during the three thermal treatments. Comparison of Fig. 6b and Fig. 8a shows that little coarsening has occurred at 700 °C: the average α plate width has increased from 0.61 μm in the as-welded condition to 0.71 μm after the 700 °C treatment. Considerable growth takes place, however, during the 870 °C treatment and still more during the duplex anneal; the α plate widths after these treatments have increased to 1.53 μm (Fig. 8b) and 3.1 μm (Fig. 8c), respectively. The difference in growth between Fig. 8b and Fig. 8c suggests that the time of treatment is also important and that appreciable growth could occur even after a period of 3 h at 870 °C.

3.3. Mechanical properties

The hardness variations on transverse sections across the welds are plotted in Fig. 9a–c and the tensile properties of the fusion zone are listed in Table II. All three welding processess are seen to result in a considerable increase in hardness and yield strength of the fusion zone. This effect is somewhat more pronounced in the case of EBW. There is a concurrent reduction in ductility in the weld metal in all the three cases. Post-weld heat treatment leads to softening, which is moderate at 700 °C and appreciable for the two high-temperature annealing treatments. The fusion zone ductility also improves considerably during post-weld treatments, with the duplex anneal yielding the maximum effect. Yield and tensile strengths decrease as expected after the thermal treatments.

The hardening of the weld zone with peaking at its centre (Fig. 9a–c) may be attributed to the difficulty of

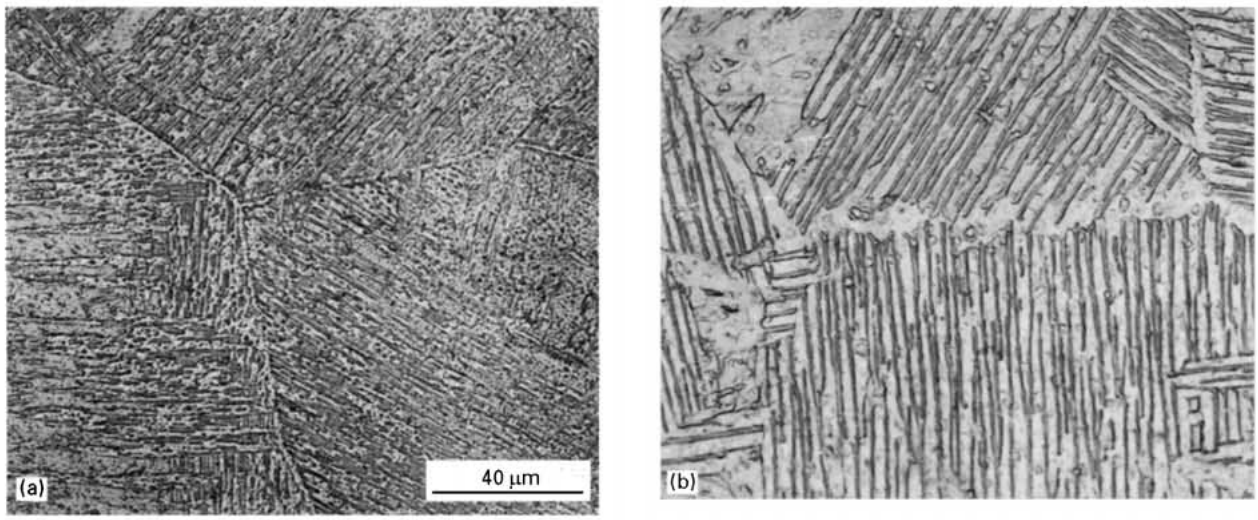

Figure 7 Light micrographs of transverse sections of electron beam weld after post-weld heat treatment: (a) after treatment at 700 °C; (b) after treatment at 870 °C.

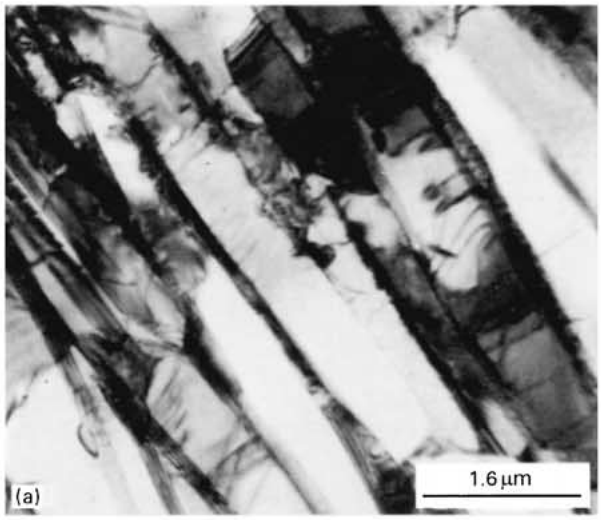

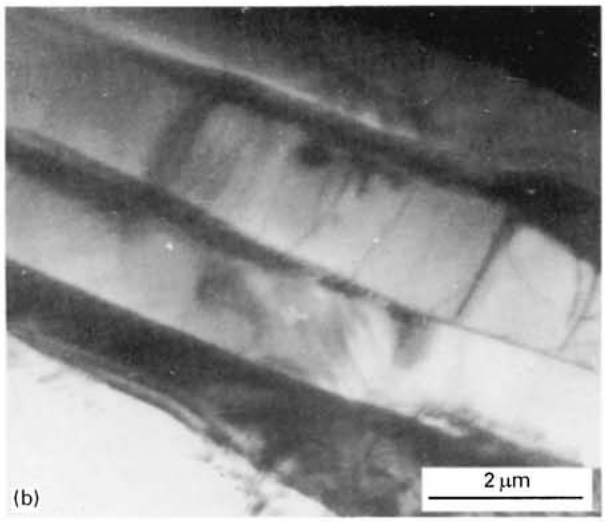

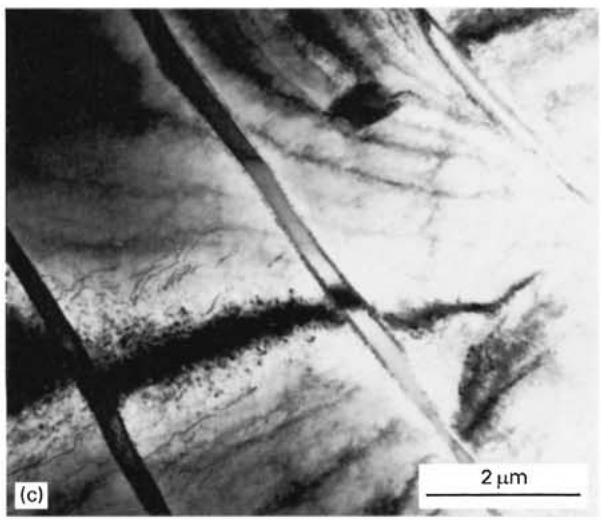

Figure 8 Transmission electron micrographs of M-GTA weld metal after post-weld heat treatment: (a) after 700 °C treatment; (b) after 870 °C treatment; (c) after duplex treatment at 870 °C + 650 °C.

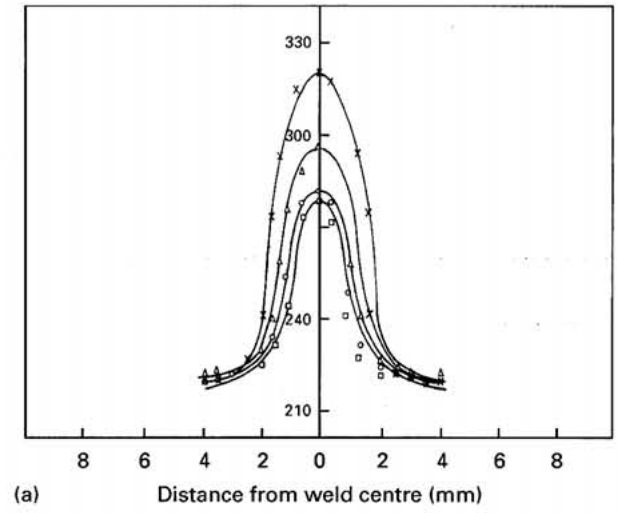

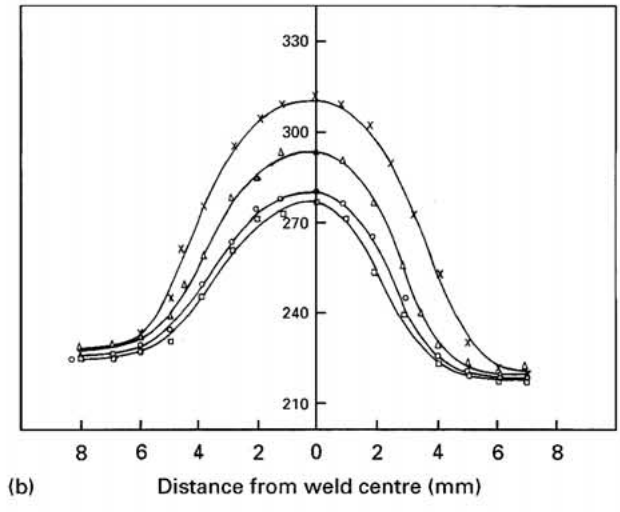

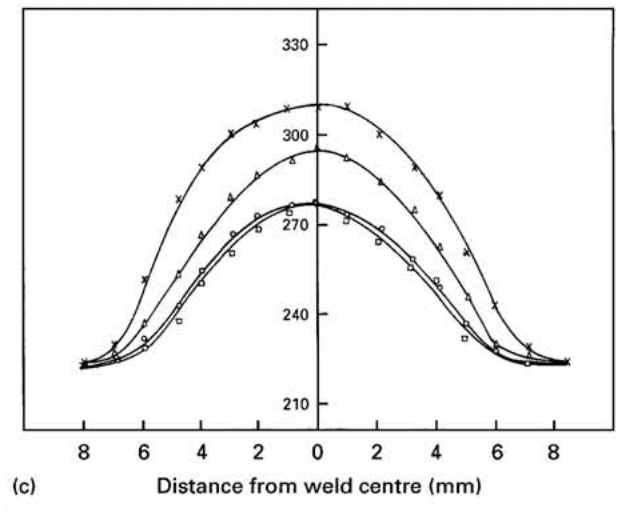

Figure 9 Vicker's hardness (5 kg load) variation across: (a) electron beam weld; (b) automatic GTA weld; (c) manual GTA weld. (×) as welded; (△) after PWHT (700 °C/3 h/FC); (○) after PWHT (870 °C/3 h/FC); (□) after PWHT (870 °C/3 h/FC + 650 °C/3 h/FC).

slip in the extremely fine, lamellar intragranular microstructure. This is in conformity with the increase in yield strength due to welding. On traversing from the weld centre into the heat-affected zone, the cooling rate becomes lower, which produces a coarser structure of reduced hardness and strength. Coarsening occurs also during post-weld annealing, which results in softening; higher temperatures and longer times of annealing lead to more pronounced coarsening and hence a greater degree of softening.

The reduction in ductility due to the weld thermal cycle is a result of the large prior-β grain size and a microstructure of high aspect ratio. The slightly greater strength of the electron beam weld may be

TABLE II Fusion zone tensile properties of OT4-1 weldments

Welding process	Conditions	Yield strength (0.2% proof stress) (MPa)	Ultimate tensile strength (MPa)	Elongation (%)
Electron beam welding	As-welded	658	771	9
	PWHT at 700 °C	555	674	15
	PWHT at 870 °C	510	637	17
	PWHT at 870 °C + 650 °C	539	652	23.5
Automatic GTAW	As-welded	608	715	9
	PWHT at 700 °C	550	670	13.5
	PWHT at 870 °C	512	629	18.5
	PWHT at 870 °C + 650 °C	523	665	20
Manual GTAW	As-welded	627	722	7
	PWHT at 700 °C	564	683	15.5
	PWHT at 870 °C	542	644	16.5
	PWHT at 870 °C + 650 °C	541	665	24

Note: 1. All results are an average of two tests each.
2. For comparison, the base material (α-β processed and annealed at 870 °C) properties were: 507 MPa (YS), 698 MPa (UTS), 25% (elongation).

ascribed to its smaller prior-β grain size and finer intragranular microstructure.

During post-weld heat treatment, the tempering of martensite has a softening effect while the ageing of the retained β phase is a hardening reaction. Overageing and grain coarsening due to prolonged heat treatment may be expected to reduce strength and increase ductility. For all three weld metals, there is a progressive softening, reduction in strength and increase in ductility during post-weld heat treatment. This implies that, for the alloy composition and the range of treatment temperatures used, the tempering of martensite is the important reaction. This is understandable because the amount of retained β phase in the as-welded condition is quite small in the dilute alloy and hardening due to precipitation cannot make an appreciable contribution. The 700 °C treatment has produced very little microstructural coarsening (Fig. 7a) unlike in the case of the high-temperature heat treatments (Fig. 7b). Nevertheless the 700 °C anneal has resulted in softening (Fig. 9a–c) and a reduction in strength (Table II) from the as-welded condition. These results suggest that overageing effects might just be beginning to occur in this alloy at 700 °C. It may be noted that the maximum ductility of the fusion zone as well as the greatest degree of softening is attained after the duplex anneal of 870 °C–3 h/FC + 650 °C–3 h/FC. The elongation is indeed comparable to that of the α-β processed base material. This demonstrates again that in structures with a lamellar morphology the highest ductility is associated with the largest alpha plate width. Void formation leading to tensile fracture is known to occur preferentially at α-β interfaces [13] and lamellar structures with a lower aspect ratio thus exhibit a greater fracture strain.

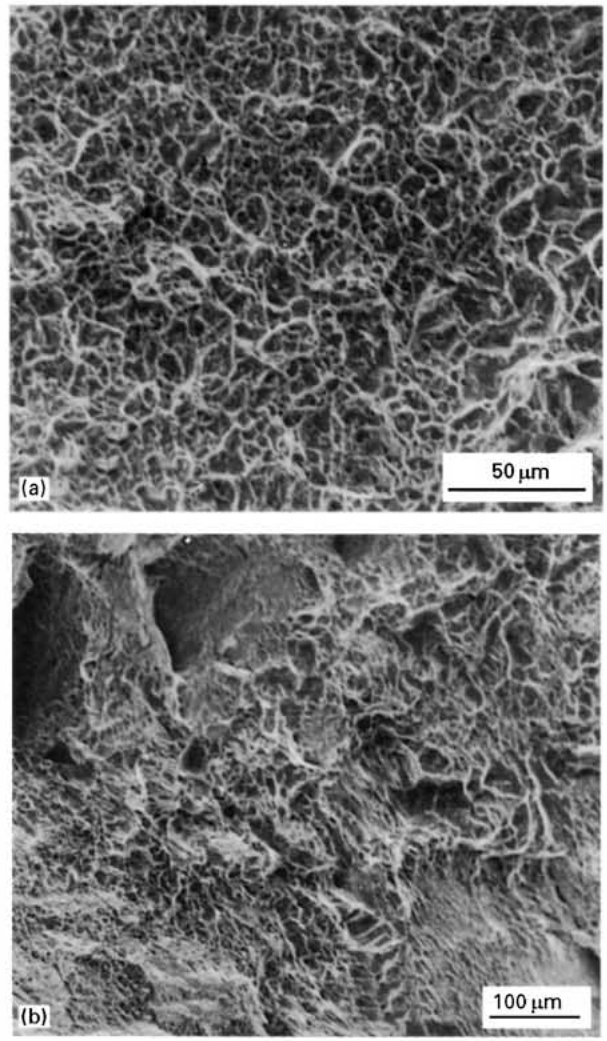

Figure 10 SEM fractographs of fusion zone tensile samples, as-welded condition: (a) electron beam weld; (b) automatic GTA weld.

3.4. Fractography

The scanning electron micrographs of the tensile fracture faces are shown in Figs 10 and 11. Differences in tensile fracture behaviour were noticed between the electron beam weld and the two GTA welds in the as-welded condition. While the electron beam weld fractured completely in a transgranular manner (Fig. 10a), the GTA weld fusion zone fracture faces

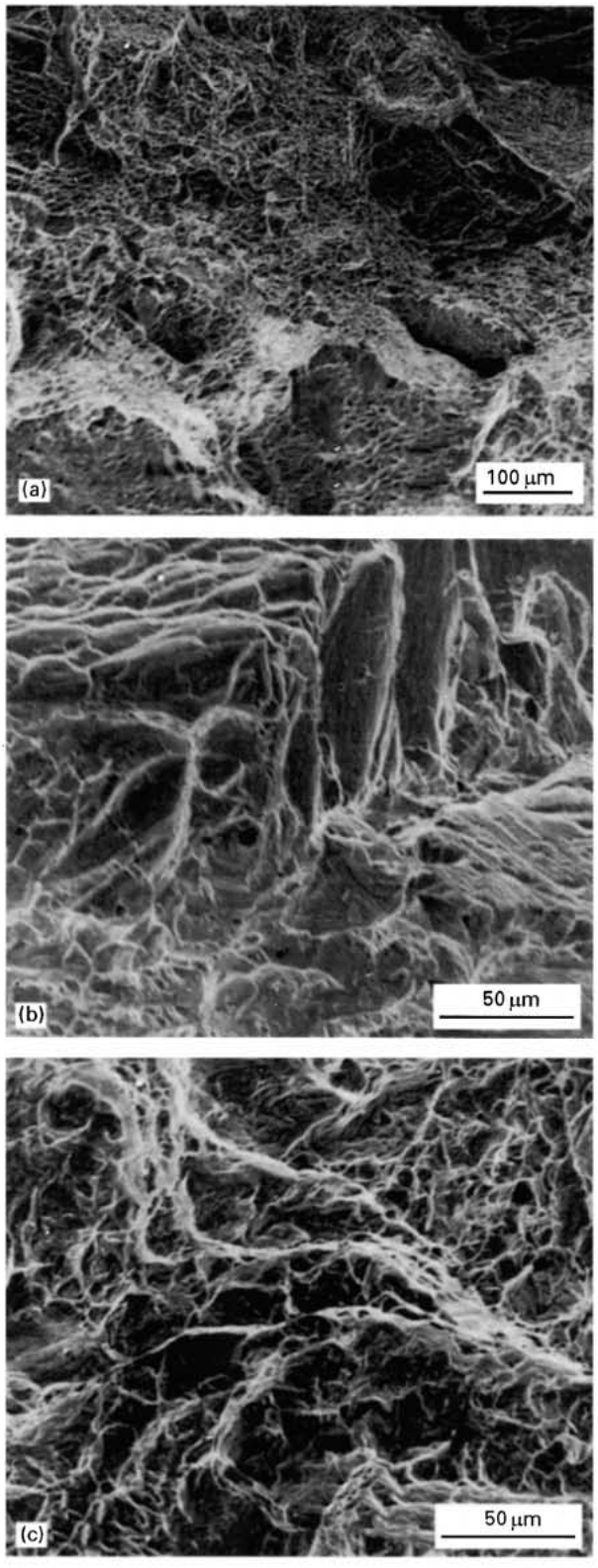

Figure 11 SEM fractographs of A-GTA weld fusion zone tensile samples after post-weld heat treatment: (a) after treatment at 700 °C; (b) after treatment at 870 °C; (c) after treatment at 870 °C + 650 °C.

showed evidence of partial intergranular rupture (Fig. 10b). This is no doubt a consequence of the grain boundary α layer present in the GTA welds in the as-welded condition. Post-weld heat treatment at 700 °C in all three cases results in tensile fracture which is also partially intergranular (Fig. 11a). However, when the heat treatment temperature is increased to 870 °C, both for the single and duplex anneals, the fracture becomes completely transgranular (Fig. 11b and c). Since the fractographs of all three fusion zones after the post-weld treatments showed similar features, they are reproduced for the A-GTA welds only.

In terms of microstructure, the treatment at 700 °C has resulted in a soft grain boundary α layer in all three welded samples and an intragranular structure that has not appreciably coarsened and softened. Slip during tensile loading is therefore confined to the grain boundary α in those grain boundary regions where the α phase is present. Slip incompatibility between grain boundary α and the harder matrix results in void formation at these boundaries, thereby promoting intergranular fracture. On the other hand, when the heat treatment temperature is raised to 870 °C, both for the single and duplex annealing treatments, the intragranular structure also becomes quite soft and no great strength difference exists between this structure and the grain boundary α. Slip is therefore more easily dispersed and fractures become predominantly transgranular. The ability for slip in the grain boundary α to be accommodated in the grain interior and the consequent occurrence of transgranular rather than intergranular cracking have also been reported in the alloy Ti–6Al–6V–2Sn [14].

Finally, it may be noted that, despite these differences, all fracture faces exhibit dimples of a variety of sizes and shapes. The fractures have therefore occurred by the usual microvoid coalescence mechanism and are microscopically ductile, even in the as-welded condition characterized by a relatively low tensile elongation.

4. Conclusions

1. Weld cooling rate plays an important role in controlling the microstructures in the fusion zone of dilute α-β titanium alloys. Rapid cooling results in a structure in which lath-type martensite predominates, while slower cooling leads to the formation of diffusion-induced products that include basketweave α-β structures, α side-plates and a grain-boundary α layer.

2. Post-weld heat treatment at 700 °C and higher temperatures eliminates the above differences in the as-welded condition and results in a lamellar α-β structure that coarsens with temperature and time.

3. The ductility lost during welding may be restored by post-weld heat treatment; prolonged annealing at a high temperature is, however, required for achieving a tensile elongation matching that of the parent material.

4. Tensile fractures are all microscopically ductile, even in conditions marked by low tensile elongation.

5. The presence of the α phase at the grain boundaries tends to promote intercrystalline fracture, especially when a hard, intragranular structure confines slip to occur in the grain boundary regions.

References

1. W. A. BAESLACK, D. W. BECKER and F. H. FROES, *J. Metals* **36** (1984) 46.

2. H. M. FLOWER, S. D. HENRY and D. R. F. WEST, *J. Mater. Sci.* **9** (1974) 57.
3. R. DAVIS, H. M. FLOWER and D. R. F. WEST, *ibid.* **14** (1979) 712.
4. W. A. BAESLACK and C. M. BANAS, *Welding J.* **60** (1981) 121s.
5. W. A. BAESLACK and F. D. MULLINS, in Proceedings of the ASM Conference on Trends in Welding Research in the United States, New Orleans, November 1981, p. 541.
6. W. A. BAESLACK, *Welding J.* **61** (1982) 197s.
7. W. A. BAESLACK and F. D. MULLINS, *J. Mater. Sci. Lett.* **1** (1982) 371.
8. K. C. WU, *Welding J.* **60** (1981) 219s.
9. U. ZWICKER, "Titan und Titanlegierungen" (Springer-Verlag, Berlin, 1974) p. 174.
10. J. C. WILLIAMS in Proceedings of the AIME Conference on Titanium Science and Technology, Vol. 3 (Plenum Press, New York, 1973) p. 1435.
11. H. M. FLOWER, P. R. SWANN and D. R. F. WEST, *J. Mater. Sci.* **7** (1972) 929.
12. B. K. DAMKROGER, G. R. EDWARDS and B. B. RATH, *Welding J.* **68** (1989) 290s.
13. J. C. WILLIAMS, J. C. CHESNUTT and A. W. THOMPSON, in Proceedings of the TMS-AIME Annual Symposium, Denver, February 1987, p. 255.
14. Y. MAHAJAN and W. A. BAESLACK, *Scripta Metall.* **13** (1979) 1125.

Received 25 March 1996
and accepted 12 September 1997